JACS
JOURNAL OF THE AMERICAN CHEMICAL SOCIETY
Article
pubs.acs.org/JACS

Origin of Stereodivergence in Cooperative Asymmetric Catalysis with Simultaneous Involvement of Two Chiral Catalysts

Bangaru Bhaskararao and Raghavan B. Sunoj*

Department of Chemistry, Indian Institute of Technology Bombay, Powai, Mumbai 400076, India

Supporting Information

ABSTRACT: Accomplishing high diastereo- and enantioselectivities simultaneously is a persistent challenge in asymmetric catalysis. The use of two chiral catalysts in one-pot conditions might offer new avenues to this end. Chirality transfer from a catalyst to product gets increasingly complex due to potential chiral match-mismatch issues. The origin of high enantio- and diastereoselectivities in the reaction between a racemic aldehyde and an allyl alcohol, catalyzed by using axially chiral iridium phosphoramidites $\mathbf{P}_{R/S}$–Ir and cinchona amine is established through transition-state modeling. The multipoint contact analysis of the stereocontrolling transition state revealed how the stereodivergence could be achieved by inverting the configuration of the chiral catalysts that are involved in the activation of the reacting partners. While the enantiocontrol is identified as being decided in the generation of $\mathbf{P}_{R/S}$–Ir–π-allyl intermediate from the allyl alcohol, the diastereocontrol arises due to the differential stabilizations in the C–C bond formation transition states. The analysis of the weak interactions in the transition states responsible for chiral induction revealed that the geometric disposition of the quinoline ring at the C8 chiral carbon of cinchona–enamine plays an anchoring role. The quinolone ring is noted as participating in a π-stacking interaction with the phenyl ring of the Ir–π-allyl moiety in the case of $\mathbf{P}_R$ with the (8*R*,9*R*)-cinchona catalyst combination, whereas a series of C–H···π interactions is identified as vital to the relative stabilization of the stereocontrolling transition states when $\mathbf{P}_R$ is used with (8*S*,9*S*)-cinchona.

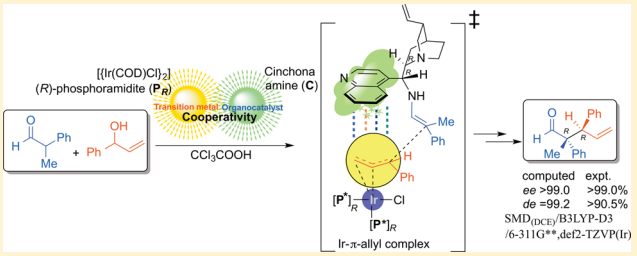

INTRODUCTION

Chirality is a fundamental property of immense importance to several life-sustaining biological recognition processes. The infamous story of thalidomide served as a shocking revelation of how different stereoisomers, such as an enantiomeric pair, can produce deleterious effects under biological conditions.[1] The contemporary significance of enantiomerically pure compounds can be readily appreciated by the fact that more than half of today's marketed drugs are chiral.[2] In addition, the use of single-enantiomer therapeutics is predicted to lead the future trends. While Nature's ability to generate single enantiomers with utmost precision continues to inspire chemists, modern asymmetric catalysis should indeed be regarded as capable of some noteworthy recipes. In particular, the domain of homogeneous asymmetric catalysis has witnessed an unprecedented growth in the last couple of decades.[3] Most of these protocols bank on ligand-controlled transition-metal catalysis[4] or make use of covalent or noncovalent activations of the reacting substrates by using small organic molecules as organocatalysts.[5]

As a natural extension of these two major approaches in asymmetric catalysis, simultaneous use of both these families of catalysts in one-pot conditions is now becoming more widespread.[6] The complementary attributes of transition-metal catalysts and organocatalysts have been harnessed in what came to be known as *cooperative catalysis*.[7] Akin to that in single-catalyst systems, gaining predictable stereocontrol in multicatalytic reactions continues to pose formidable challenges. While enantiocontrol became increasingly more amenable with the advent of superior chiral catalysts, realizing high diastereoselectivity without any erosion in the enantioselectivity still remains as a major obstacle. Improved mechanistic understanding would provide a timely impetus to the concept and practice of asymmetric multicatalytic reactions.[8] There have been a few interesting experimental reports that employed two chiral catalysts in one-pot conditions.[9,13f,14] However, studies focusing on the origin of stereoinduction when two chiral catalysts are used together have not been reported to date.

Although a good number of interesting examples on cooperative asymmetric catalysis have appeared in the recent times, the most promising variant appears to employ a combination of enamine (organocatalyst) and transition-metal catalysis.[10] Over the years, the cinchona family of amines has been used as a bifunctional asymmetric organocatalyst.[11] Similarly, the use of iridium–π-allyl complexes in allylation reactions constitutes an important protocol in transition-metal catalysis.[12,13] Hence, a catalytic partnership that thrives on the catalytic attributes of enamine and Ir–π-allyl is of inherent interest as a cooperative asymmetric catalytic dyad. Indeed, a

Received: June 12, 2015
Published: November 23, 2015

DOI: 10.1021/jacs.5b05902
J. Am. Chem. Soc. 2015, 137, 15712–15722

Scheme 1. Representative Example of an α-Allylation Reaction Using a Cooperative Asymmetric Dual Catalytic Method Employing a Chiral Phosphoramidite (P1) and Cinchona (C1)

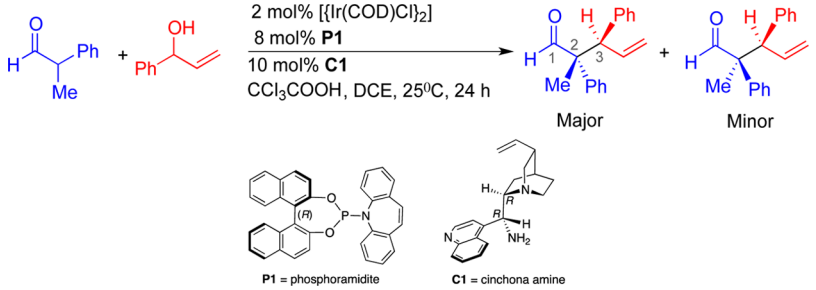

very recent report from the Carreira group offered a landmark example of an asymmetric dual catalytic approach toward the creation of two contiguous chiral carbon atoms (Scheme 1).[14] The mechanistic picture is expected to be more complex owing to the participation of two chiral catalysts and hence throws open some fundamental questions on chirality transfer. To this end, molecular understanding of the stereoelectronic origin of enantio- and diastereo-control is vital. At the heart of such catalytic processes is *stereoinduction*, wherein the transfer of chiral information from the chiral catalyst to the product occurs through the stereocontrolling transition state.[15] The studies on transition states have been an invaluable tool toward establishing the origin of enantio- and diastereoselectivities in a gamut of diverse reactions besides aiding in rational catalyst design.[16] In this paper, we present (a) mechanistic insights on cooperativity in this dual catalytic reaction and (b) the molecular origin of stereodivergence leading to stereochemically unique products obtained upon altering the catalyst combination.

COMPUTATIONAL METHODS

Computations were performed using Gaussian09 (Revision D.01) suite of quantum chemical program.[17] The geometries were optimized using the B3LYP-D3 hybrid density functional theory[18] using Pople's 6-31G** basis set for all atoms except iridium. The Los Alamos pseudopotential (LANL2DZ) basis set consisting of an effective core potential (ECP) for 60 core electrons and a double-ζ quality valence basis set for 17 valence electrons was employed for Iridium atom.[19] All of the stationary points were characterized as minima or a first-order saddle point (transition states) by evaluating the corresponding Hessian indices. The transition states were verified by examining whether it has a unique imaginary frequency representing the desired reaction coordinate. Intrinsic reaction coordinate (IRC) calculations were additionally carried out to further characterize the true nature of the transition states.[20] The geometries obtained as the end points on either side of the IRC trajectories were subjected to further optimization to identify the reactant and product that arise from the transition state. The effect of a solvent continuum, in dichloroethane (DCE), was evaluated using the Cramer–Truhlar continuum solvation model that employs quantum mechanical charge densities of solutes, designated as SMD.[21] The zero-point vibrational energy (ZPVE) and thermal and entropic corrections obtained at 298.15 K and 1 atm pressure derived from the gas-phase computations at the B3LYP-D3/6-31G**,LANL2DZ(Ir) level of theory have been applied to the "bottom-of-the-well" energies obtained from the single-point energy evaluations in the solvent phase at the $SMD_{(DCE)}$/B3LYP-D3/6-311G**,def2-TVZP(Ir) level of theory to estimate the Gibbs free energies of solutes in the condensed phase. The discussions in the text are presented using the $SMD_{(DCE)}$/B3LYP-D3/6-311G**,def2-TVZP-(Ir)//B3LYP-D3/6-31G**,LANL2DZ(Ir) level of theory, unless otherwise specified.[22] In addition, B3LYP[23] and M06[24] functionals were used as well for the optimization of different likely active catalysts.[32] Dehydroxylation of alcohol was examined by using the B3LYP functional, in addition to the B3LYP-D3.[35] Graphical representations of the optimized geometries were created by using CYLView.[25]

Topological analyses of electron densities were carried out using Bader's Atoms-in-Molecule formalism wherein bond paths and bond critical points are identified.[26] Analyses of noncovalent interactions were carried out using noncovalent interaction index (NCI) as proposed by Yang and co-workers.[27] The Gibbs free energies of the C–C bond formation transition states were employed in estimating the Boltzmann distribution, which in turn, was used in the computation of the enantiomeric and diastereomeric excesses in accordance with the following equation.[28] Using the following equation, %ee can be computed, if $\Delta G^{\ddagger}$, which is the difference in the Gibbs free energies between the diastereomeric transition states, is known.

$$\text{ee} = \frac{1 - e^{-\Delta G^{\ddagger}_{R/S}/RT}}{1 + e^{-\Delta G^{\ddagger}_{R/S}/RT}} \times 100$$

RESULTS AND DISCUSSION

The present reaction is characterized by a number of interesting features such as an effective diastereo- and enantiocontrol over the newly formed α and β chiral carbon atoms (C_2 and C_3 atoms, Scheme 1). Four catalyst combinations, generated by using **P1** or **P2** in conjunction with **C1** or **C2**, have been independently employed to demonstrate that the desired stereodivergence could indeed be achieved wherein all four stereoisomers were generated (Scheme 3). While **P1** and **P2** phosphoramidites, respectively, have *R* and *S* axial chirality, **C1** and **C2**, respectively, represent 8*R*,9*R* and 8*S*,9*S* configurations of the cinchona catalyst. The catalyst combination such as **P1**–**C1** therefore indicate the use of (*R*)-phosphoramidite with (*R*,*R*) cinchona, and **P2**–**C2** represent the use of (*S*)-phosphoramidite with (*S*,*S*) cinchona. It is important to note that only one chiral Ir–bis-phosphoramidite ($[Ir(Cl)(\mathbf{P})_2]$) complex and one cinchona catalyst are employed together at a time in this reaction. In addition to the mechanism and stereodivergence of this reaction, the question of how two chiral catalysts work in concert, surmounting the chiral *match–mismatch* issue, is profoundly important. The Results and Discussion is organized in three subsections, each focusing on some of the important mechanistic or stereochemical features of this reaction.

1. Activation of Reactants through the Formation of Key Intermediates. The reactants aldehyde and allyl alcohol can be activated, respectively, by the cinchona and Ir–phosphoramidite catalysts under the given reaction condition. The activation of aldehyde is identified to proceed through a multistep mechanism involving a condensation reaction with

DOI: 10.1021/jacs.5b05902
J. Am. Chem. Soc. 2015, 137, 15712–15722

Scheme 2. Formation of (a) Enamine between the Catalyst Cinchona and Reactant Aldehyde and (b) Activation of Allyl Alcohol by [Ir(Cl)(bis)-phosphoramidite] Leading to Ir−π-Allyl Complexes[a]

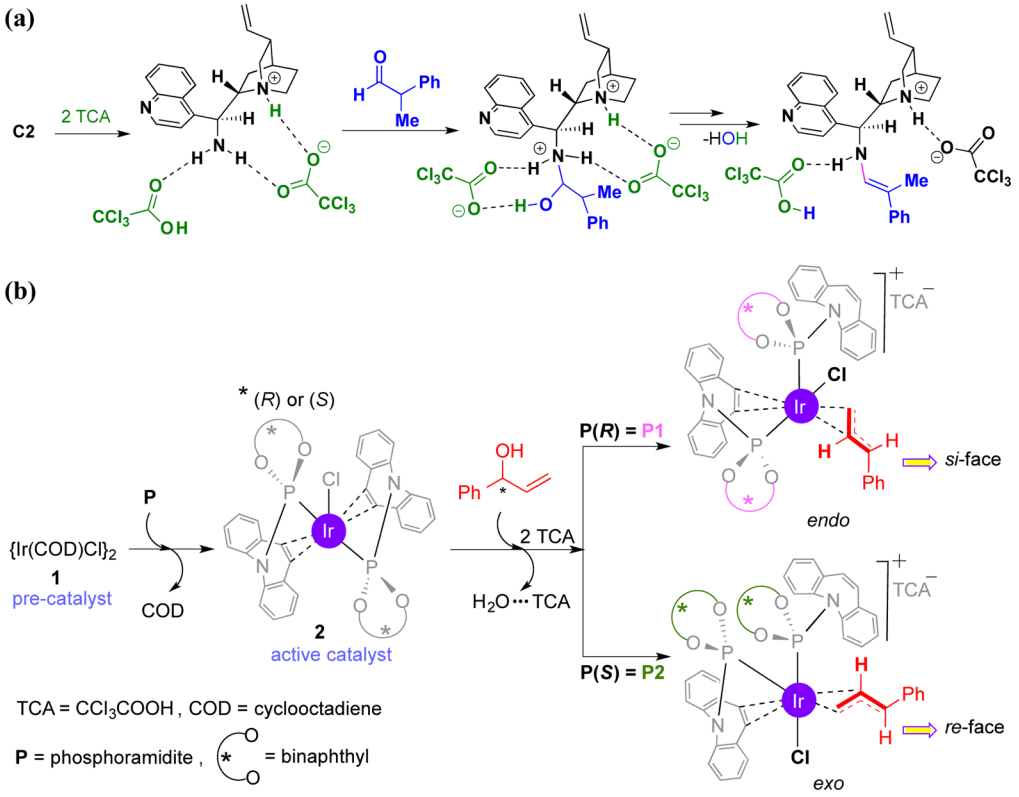

[a]Only a representative diastereomer of the Ir−π-allyl complex for each phosphoramidite (**P1** or **P2**) is shown.

the primary amine moiety of the cinchona catalyst (Scheme 2(**a**)). The computed energetics revealed an active participation of two molecules of trichloroacetic acid, which is a vital additive in this reaction.[29] We have considered different conformers of both the parent cinchona as well as that for the cinchona enamine. The most preferred conformer of the cinchona enamine is subsequently employed in the stereocontrolling C−C bond formation.[30]

In line with the commonly proposed mechanisms involving a dimeric chloro-bridged catalyst precursor [{Ir(COD)Cl}$_2$], the dissociation into a monomer followed by an exchange of the COD (cycloocta-1,5-diene) ligand with the chiral phosphoramidite (**P**) is considered here.[13b,31] It is identified that a bis-phosphoramidite [Ir(Cl)(**P**)$_2$] is the most likely active species wherein the iridium atom is coordinated to phosphorus and the olefin of the dibenzazepine moieties from each of the bound phosphoramidite ligands (Scheme 2(**b**)).[32] Further credence to this proposal that [Ir(Cl)(**P**)$_2$] would serve as the active catalyst comes from the availability of crystal structures.[33] It is of importance to describe here that we have carefully sampled a fairly large number of conformers as well as configurations of this bis-phosphoramidie iridium chloride complex. While more details can be found in the Supporting Information (Figure S1), herein we wish to provide some implicit details to convey that the lowest energy [Ir(Cl)(**P**)$_2$] species has been used in the present study. Depending on the relative dispositions of the ligands around iridium (π-allyl, chloride, and phosphoramidites - with two major binding modes, the one (i) involving both phosphorus and π-olefin moiety of the dibenzazipine, or the other (ii) only through the phosphorus) several configurations are first examined. The lower energy complexes exhibited a general preference toward a *trans* arrangement between the chloro and the phosphorus of the phosphoramidite ligand (refers to the phosphoramidite which is bound to iridium, both through the phosphorus and the π-olefin moiety). Within each such configuration, permissible bond rotations, particularly around the Ir-phosphorus bond of the phosphoramidite ligand and the P−N bond within the phosphoramidite ligand are considered as well.[34]

The uptake of the allyl alcohol by the active catalyst is facilitated by the displacement of one of the olefin coordinations of the phosphoramidite, as shown in Scheme 2(**b**). The generation of Ir−π-allyl intermediate can then be accomplished by protonating the Ir-bound-allyl alcohol and an ensuing removal of a molecule of water. We notice that explicit participation of two trichloroacetic acid (TCA) molecules is critical to substrate activation, both in the dehydroxylation of the allyl alcohol[35] and in the formation of cinchona enamine.[36] Herein we use *R*-phosphoramidite (**P1**) as a representative chiral ligand on iridium to disclose some molecular level insights on the formation of Ir−π-allyl intermediates. Interestingly, the first chiral recognition in the mechanistic course of this reaction occurs between [Ir(Cl)(**P1**)$_2$] and the *R*-allyl alcohol present in the racemic mixture. A shape-selective chiral recognition is noticed in the catalyst-substrate interaction as well as in the ensuing dehydroxylation transition states leading to the Ir−π-allyl intermediates.[37] The manifestation of chiral recognition can be readily gleaned from the relative Gibbs free energies of the intermediates and the transition states involved in the formation of Ir−π-allyl intermediates as shown in Figure 1(**a**). The initial recognition complex between the catalyst iridium-phosphoramidite (**P1**) and allyl alcohol

DOI: 10.1021/jacs.5b05902
J. Am. Chem. Soc. 2015, 137, 15712−15722

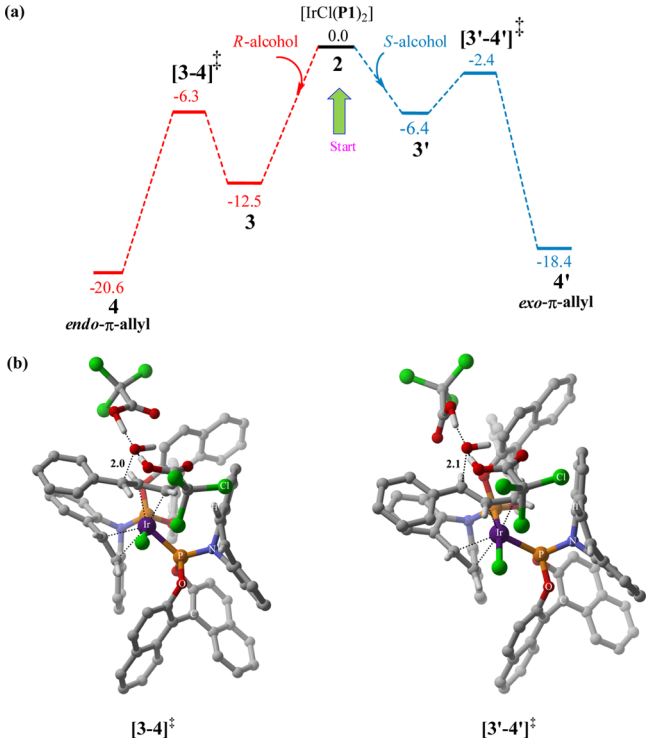

Figure 1. (a) Gibbs free energy profile for the likely formation of *endo* and *exo* Ir−π-allyl intermediates respectively from *R* and *S* allyl alcohol with **P1** (= **P**(*R*)) as the chiral ligand on iridium. Gibbs free energy profile (in kcal/mol) obtained at the $SMD_{(DCE)}$/B3LYP-D3/6-311G**,def2-TZVP(Ir)//B3LYP-D3/6-31G**,LANL2DZ(Ir) level of theory. (b) Corresponding transition-state geometries for dehydroxylation.

exhibits a thermodynamic preference for the formation of a complex between *R*-alcohol and (*R*)-phosphoramidite (**P1**) by about 6 kcal/mol as compared to that between *S*-alcohol and **P1**. Furthermore, the Gibbs free energy of the transition state for dehydroxylation of the *R*-alcohol is 3.9 kcal/mol lower than that from the *S*-alcohol. The transition state geometries for the formation of Ir−π-allyl intermediates are provided in Figure 1(**b**), particularly to emphasize the fact that in the lower energy transition state, C2−H of the allyl fragment is *anti* to the Ir−Cl bond, suggesting the formation of an *endo* Ir−π-allyl intermediate.

More important aspect of the aforementioned TCA-assisted alcohol dehydroxylation under the chiral environment is that the *R*-allyl alcohol exclusively renders an *endo* configuration to the resulting Ir−π-allyl intermediate when the chiral ligands on the iridium center are (*R*)-phosphoramidites. The *endo* or *exo* configurational descriptors of the Ir−π-allyl moiety, as depicted in Scheme 2, pertain to the open prochiral face available for the reaction with the incoming nucleophile. In the case of (*R*)-phosphoramidite (**P1**), an *anti* orientation of the C2−H and the Ir−Cl bond is denoted as *endo* (which offers the *si*-face) whereas the corresponding *syn* orientation is termed as *exo*. However, with (*S*)-phosphoramidite (**P2**), the *anti* orientation of the C2−H and Ir−Cl bonds is taken as *exo* (offers the *re*-face) and *syn* orientation as *endo*. These geometric features of the Ir−π-allyl complexes are acutely relevant to stereochemical outcome of the reaction, as the *endo* and *exo* intermediates respectively offer only the *si* and *re* prochiral faces for the ensuing C−C bond formation. This stereochemical feature is reminiscent of *chiral memory effect* wherein the *R*-allyl alcohol translates to *endo*-Ir-π-allyl intermediate, which subsequently reacts with the incoming nucleophile only through its open *si* face. The decision as to what the configuration of the phenyl bearing carbon (i.e., β-carbon in the product) would be is made in this very step, which in turn, depends on the chirality of the phosphoramide involved.

The above-mentioned chiral recognition and dehydroxylation of the iridium-bound allyl alcohol is a good model toward understanding the formation of one of the diastereomeric Ir−π-allyl intermediates (*endo* or *exo*), depending on the chirality of the phosphoramidite involved. Another noteworthy feature at this juncture is that the yield of the major stereoisomer formed in the reaction is in the range of 75 to 85%, indicating that both *R* and *S* enantiomers of the racemic alcohol are indeed converted to the final product. In other words, during the course of the reaction, the racemic alcohol converges to one diastereomeric form of the Ir−π-allyl intermediate. To illustrate this point further, herein we take the combination of *R*-phosphoramidite on iridium and racemic allyl alcohol. Two key coordination modes of the allyl alcohol to $[Ir(Cl)(\mathbf{P1})_2]$ can be envisaged as shown in Figure 2. It can be noticed that in configurations $\mathbf{c}_R$ and $\mathbf{c}_S$, the hydroxyl group is oriented toward the open face and hence the approach of the trichloroacetic acids is expected to be easier. Further, the *anti* orientation of the C2−H and the Ir−Cl bond in $\mathbf{c}_R$ in the case of *R*-allyl alcohol conveys that the ensuing Ir−π-allyl intermediate would present an *endo* configuration. A similar process from the *S*-allyl alcohol could furnish only *exo* Ir−π-allyl intermediate via configuration $\mathbf{c}_S$.

A more important aspect relates to the other possible configurations denoted as $\mathbf{c}'$, as shown in the second row of Figure 2.[38] Here, the orientation of the hydroxyl group is toward a more crowded region and hence not conducive for the approach of the TCA to facilitate the dehydroxylation process. However, if dehydroxylation can be achieved from this configuration ($\mathbf{c}'_S$), the *S*-allyl alcohol can as well provide access to the desired *endo* Ir−π-allyl intermediate. However, the Gibbs free energy of the dehydroxylation transition state from configuration $\mathbf{c}'_S$ is found to be higher by 15.8 kcal/mol than that from configuration $\mathbf{c}_R$.[39]

Under this circumstance, we have examined an alternative mechanistic route wherein a hydronium ion (generation by the action of TCA on water, which could be considered as present in trace quantities either in the reagents or the one formed as a result of the initial condensation between the cinchona amine and the aldehyde) acts as the promoter for dehydroxylation as shown in Figure 3. Interestingly, the elementary step barrier for the H_3O^+ assisted dehydroxylation of *S*-allyl alcohol is 5.6 kcal/mol as opposed to 12.9 kcal/mol for the corresponding TCA assisted pathway, both from conformer $\mathbf{c}'_S$. It is noted that the approach of the H_3O^+ to the hindered face of the allyl alcohol is easier as it can come closer to the hydroxyl group. However, in the case of TCA-assisted dehydroxylation from conformer $\mathbf{c}'_S$, the N-olefin coordination of the benzazipine is found to open up when one of the TCA molecules transfers its proton to the hydroxyl group. The open coordination site on the iridium is subsequently occupied by the trichloroacetate.[39,40] Through this alternative route, the *endo* Ir−π-allyl intermediate could be generated, providing a convergence to one single diastereomeric Ir−π-allyl intermediate. We propose that the origin of stereoconvergence to *endo* Ir−π-allyl intermediate arises due to an energetically affordable alternative dehydroxylation pathway

DOI: 10.1021/jacs.5b05902
J. Am. Chem. Soc. 2015, 137, 15712−15722

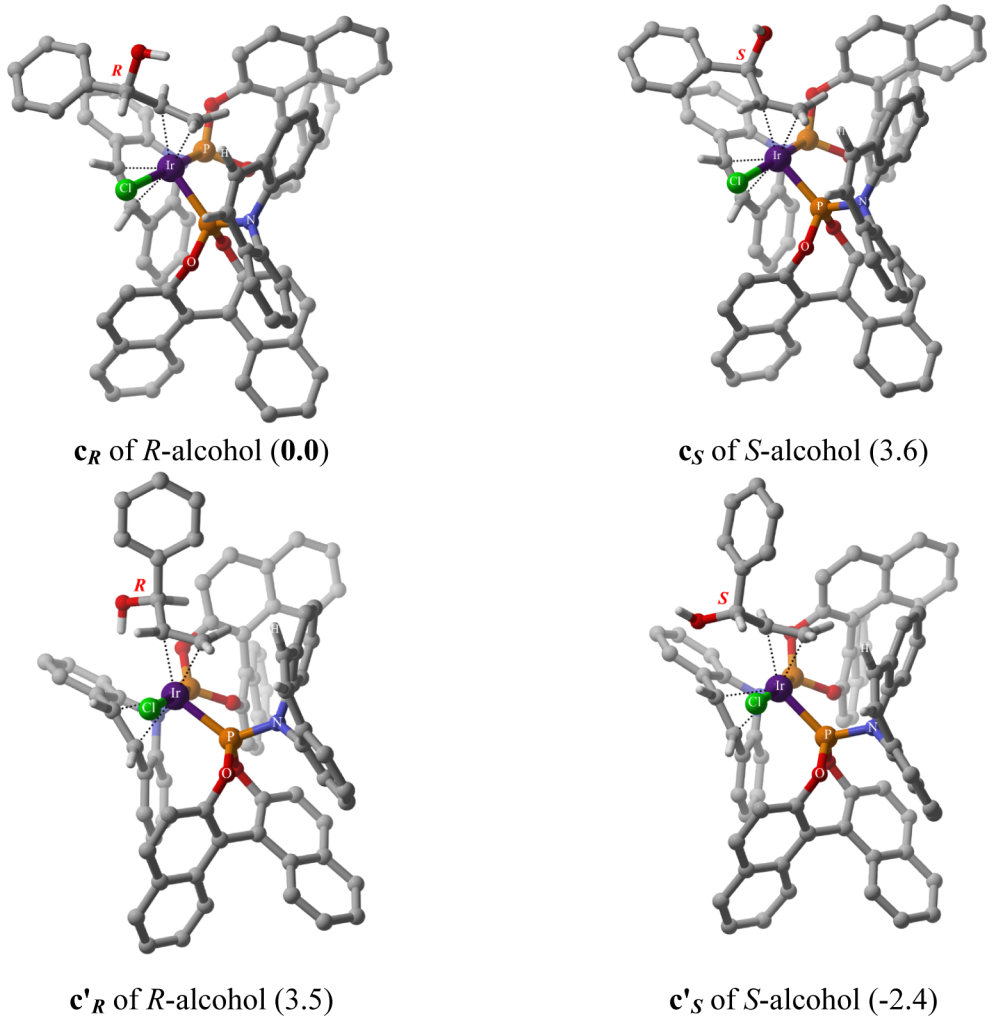

Figure 2. Two important configurations of $[IrCl(\mathbf{P1})_2]$ allyl alcohol complexes and the corresponding relative Gibbs free energies (in kcal/mol). In configuration **c** the hydroxyl group remains in a relatively more open top face than in configuration **c**′, where the hydroxyl group is in a more hindered bottom face.

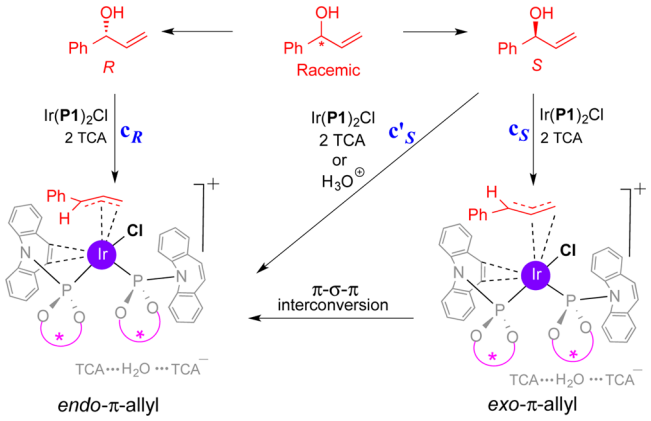

Figure 3. Different possibilities for the stereoconvergent formation of the *endo* Ir−π-allyl intermediate with *R*-phosphoramidite (**P1**) ligand on iridium.

for the *S* enantiomer of the racemic alcohol via conformer $\mathbf{c'}_S$ and a normal pathway for *R* alcohol via conformer $\mathbf{c}_R$.

Another seemingly obvious possibility for the formation of a single diastereomer *endo* Ir−π-allyl intermediate from the racemic alcohol with *R*-phosphoramidite ligand is to invoke an interconversion pathway. Here, the *S*-alcohol should first proceed through a higher energy dehydroxylation pathway (via the $\mathbf{c}_S$ conformer) to yield its natural *exo* Ir−π-allyl intermediate. This could then follow a $\pi-\sigma-\pi$ interconversion transition state to the lower energy *endo* Ir−π-allyl intermediate.[41] We note that the interconversion pathway is more energy demanding as revealed by a higher energy transition state, as compared to the H_3O^+ assisted dehydroxylation route. Thus, far, the discussions focused on stereoconvergent formation of *endo* Ir−π-allyl intermediate from the racemic alcohol when $[Ir(Cl)(\mathbf{P1})_2]$ acts the catalyst.

2. Reaction between Nucleophile (Cinchona−Enamine) and Electrophile ($[Ir(Cl)(\pi\text{-allyl})(P)_2]$): The Carbon−Carbon Bond Formation. The activated substrates, namely, cinchona−enamine and $[Ir(Cl)(\pi\text{-allyl})(\mathbf{P})_2]$ species, can now react to form a new C−C bond leading to two chiral carbon atoms. Convergence of organo and transition-metal catalytic cycles occur in this stereocontrolling C−C bond formation step wherein both nucleophilic and electrophilic partners react through their prochiral faces.[42] Within each of these stereochemical modes, the most preferred transition-state model for the C−C bond formation is identified through a detailed sampling of possible conformers and configurations. These possibilities arise due to permissible bond rotations within a

DOI: 10.1021/jacs.5b05902
J. Am. Chem. Soc. 2015, 137, 15712−15722

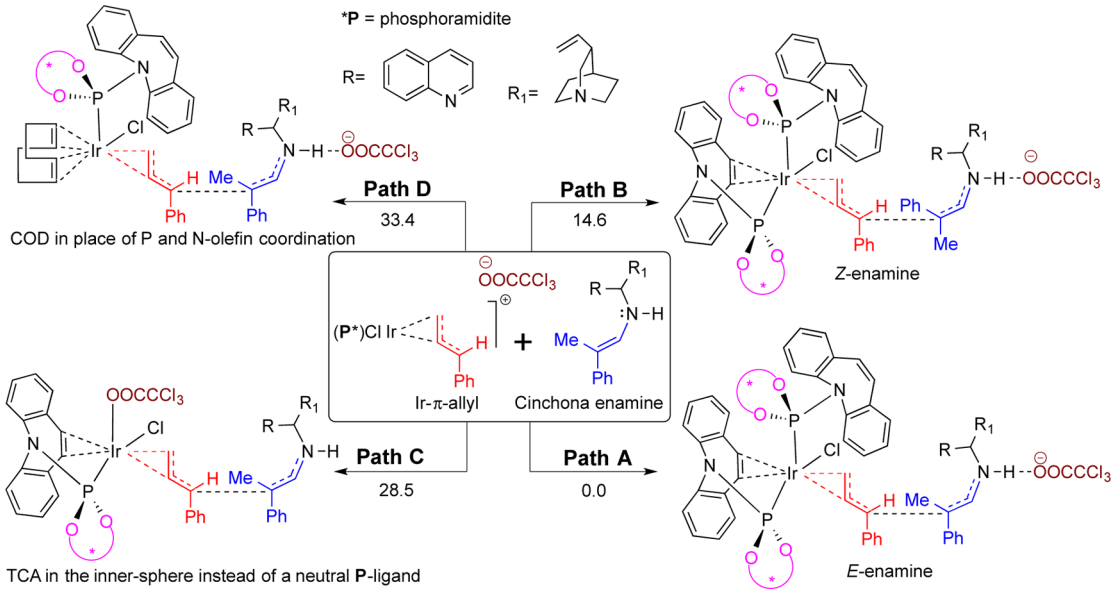

Figure 4. Different possibilities for the stereocontrolling C−C bond formation transition states and the corresponding relative Gibbs free energies (in kcal/mol).

Scheme 3. Different Likely Approaches between the Prochiral Faces of Cinchona−Enamine and Ir−π-Allyl(bis)-phosphoramidite in the Stereocontrolling C−C Bond Formation[a]

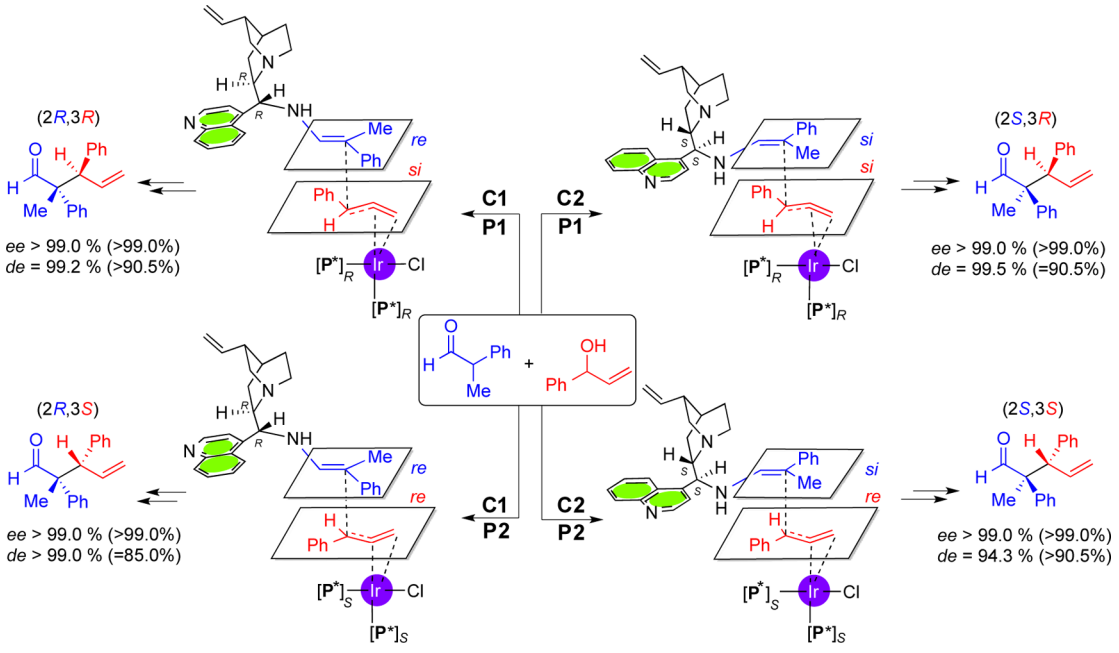

[a]Stereodivergence leading to the formation of different stereoisomers and the computed enantio- and diastereo-selectivities are given. Experimental values[14] of ee and de are provided in parentheses.

ligand arrangement around the metal center as well as varying relative dispositions of the ligands within a given configuration, respectively.[34,43] A representative set of such possibilities for the C−C bond formation is provided in Figure 4. Of the four modes shown in Figure 4, the bis-phosphoramidite combination is found to be of lower energy (paths A and B) than when other ligands such as COD and trichloroacetate are bound to the iridium (paths C and D). In the most preferred transition-state model for the C−C bond formation, [Ir(Cl)(π-allyl)(**P**)$_2$] acts as the electrophile and cinchona enamine in its *E*-configuration is the nucleophilic partner (path A).

After having identified the preferred ligand combination and the geometric preferences of the reacting partners, we turned our attention to the key question of how chirality at the developing chiral centers is induced by the simultaneous action of two chiral catalysts. An illustration of this stereocontrolling event is provided in Scheme 3 by using a representative case for each catalyst combination examined in this study.

The computed relative energies of the C−C bond formation transition states across all the stereochemically distinct modes for all catalyst combinations are provided in Table 1. For each catalyst combination, the lowest energy transition state energy

DOI: 10.1021/jacs.5b05902
J. Am. Chem. Soc. 2015, 137, 15712−15722

Table 1. Relative Gibbs Free Energies of Solvation (in kcal/mol) for the C−C Bond Formation Transition States between the Prochiral Faces of the Nucleophile and the Electrophile Obtained at the SMD$_{(DCE)}$/B3LYP-D3/6-311G,def2-TZVP(Ir)//B3LYP-D3/6-31G**,LANL2DZ(Ir) Level of Theory for Different Catalyst Combinations (Phosphoramidite (P) and Cinchnoa (C))[44]**

nucleophile−electrophile	product configuration	P1−C1	P1−C2	P2−C1	P2−C2
re−*si*	(2*R*,3*R*)	**0.0**	3.6	5.7	6.9
si−*si*	(2*S*,3*R*)	3.3	**0.0**	12.3	10.2
si−*re*	(2*S*,3*S*)	7.6	5.2	4.5	**0.0**
re−*re*	(2*R*,3*S*)	11.3	8.2	**0.0**	2.1

is set as zero, which is indicated in bold font type in the table. It can be noticed that with the **P1−C1** catalyst combination the addition of the *re*-face of the cinchona−enamine to the *si*-face of the Ir−π-allyl species is found to be the most preferred mode. Such an approach will lead to the final product with a (2*R*,3*R*) configuration. On the other hand, addition of the *si*-face of enamine to the *re*-face of the electrophile for the formation of the enantiomeric product is about 7.6 kcal/mol higher in energy, indicating a kinetic advantage and an enantiomeric excess of >99% in favor of the (2*R*,3*R*) product. The computed data therefore suggest an exclusive formation of only one enantiomer, which was precisely what Carreira and co-workers noted earlier.[14] Similarly, the transition state responsible for the formation of the (2*S*,3*R*) diastereomer via the addition of the *si*-face of enamine to the *si*-face of the Ir−π-allyl species is found to be 3.3 kcal/mol higher than the *re*−*si* mode of addition. This large energy separation corresponds into a diastereomeric excess of more than 99%. In general, the predicted enantioselectivities are found to be in superior agreement with the experimental observations (as all the % ee's are >99), while the predicted diastereoslectivities exhibited a modest overestimation (Scheme 3). In other words, the computed energies of the transition states can effectively be used to rationalize the observed stereodivergence achieved by suitable catalyst combination.

An interesting stereochemical outcome of this reaction with [Ir(Cl)(**P1**)$_2$] (a representative catalyst here) is that in both major (2*R*,3*R*) and minor (2*S*,3*R*) products the configuration at the C3 carbon is *R*, indicating that the Ir−π-allyl electrophile reacts with the nucleophilic enamine (**C1** here) exclusively through its *endo* configuration. Formation of the major and minor diastereomers arises due to the difference in the prochiral faces of the enamine that adds to the *endo* Ir−π-allyl intermediate. In fact, Carreira and co-workers have noticed no trace of products with a 3*S* configuration in their HPLC profiles.[14] The preferential formation of *endo* Ir−π-allyl intermediate from the racemic alcohol with [Ir(Cl)(**P1**)$_2$] as the catalyst is quite likely. While experiments by the Carreira and the Helmchen groups[12c,13c] have indicated a potential equilibrium between *endo* and *exo* π-allyl intermediates, Hartwig and co-workers have showed using a related family of chiral phosphoramidite ligands that the reaction of Ir−π-allyl intermediate with a nucleophile is faster than the *endo*−*exo* interconversion.[13j] Our computational model described hitherto in this manuscript revealed a direct conversion of *R*-alcohol and an H_3O^+-assisted route for the *S*-alcohol, both converging to a common *endo* Ir−π-allyl intermediate. This model is in line with the experimental observation that only two diastereoisomers, namely (2*R*,3*R*) as the major and (2*S*,3*R*) as the minor product, are formed.

A modest overestimation of the noncovalent interactions present in these stereocontrolling transition states (vide infra) appears to result in a slightly higher computed diastereoselectivities as compared to that of the experimentally observed values. Quantitatively accurate predictions on stereoselectivity continue to remain a key challenge in transition-state modeling with larger catalyst−substrate combinations, such as in the present study. Similar overestimation of enantio- and diastereoselectivities has been noticed previously with the use of dispersion-corrected B3LYP functional in asymmetric catalysis.[45]

The effectiveness of stereodivergence as well as its energetic origin can be appreciated by examining the transition state energies of another catalyst combination such as **P2−C1**, wherein only the Ir−π-allyl phosphoramidite configuration is inverted to *S* while cinchona is retained in the 8*R*,9*R* configuration (Table 1). The lowest energy stereochemical mode of addition in the case of *R*,*R* cinchona−enamine to Ir−π-allyl-(*S*)-phosphoramidite is identified to involve the *re*-face of enamine and the *re*-face Ir−π-allyl. Such a preference for the approach of the prochiral faces of the reacting partners will result in a product configuration of (2*R*,3*S*). In other words, the configuration of the β-carbon can be inverted to *S* by changing

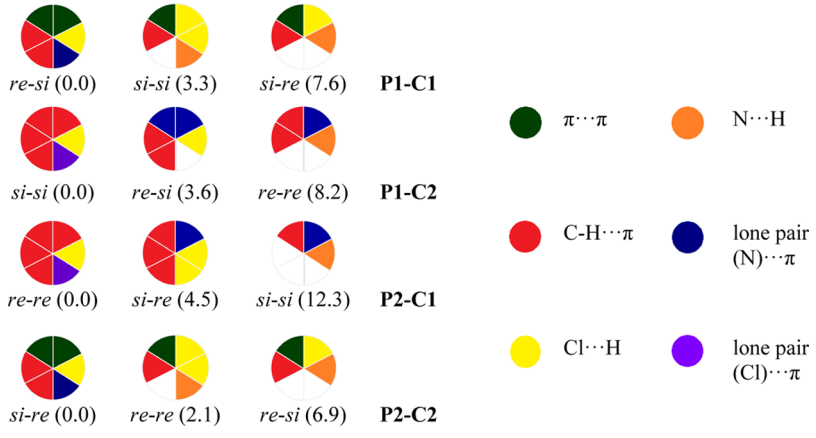

Figure 5. Interaction wheel model for noncovalent interactions in the stereocontroling transition states and the corresponding relative Gibbs free energies of solvation (in kcal/mol) for all catalyst combinations as compiled in Table 1.

DOI: 10.1021/jacs.5b05902
J. Am. Chem. Soc. 2015, 137, 15712−15722

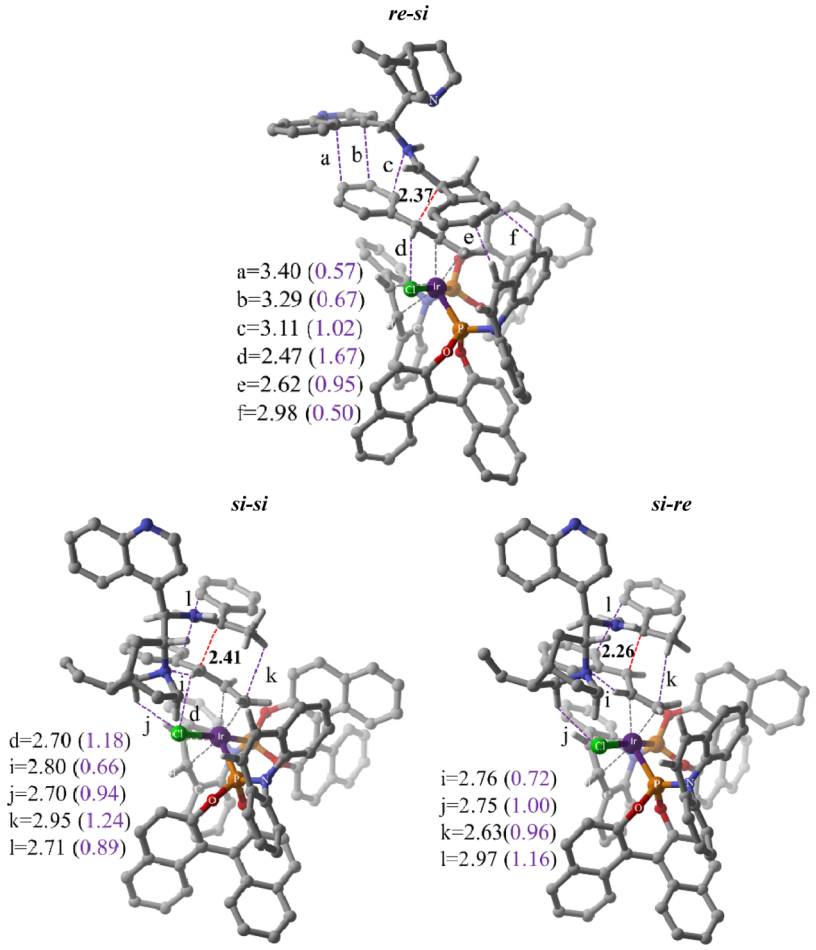

Figure 6. Optimized geometries of the stereocontroling transition states in the case of **P1−C1** catalyst combination. For improved clarity, TCA counterion and a few hydrogen atoms are omitted. All distances are in angstroms. Values in parentheses are electron densities at the bond critical points along the bond paths (ρ*10^{-2} au).

the chirality of the Ir−π-allylphosphoramidite. In the case of **P2−C1** catalyst combination, the predicted stereoselectivities are rather overestimated compared to other examples presented herein.

Equally important is examination of the energetic reordering of the stereocontrolling transition state when 8*S*,9*S* cinchona−enamine (**C2**) is used with Ir−π-allyl-(*R*)-phosphoramidite (**P1**). The lowest energy transition state with this combination turns out to be for the *si*−*si* mode of addition, leading to a product configuration of (2*S*,3*R*). This prediction indicates that the configuration of the α-carbon can be inverted by choosing the 8*S*,9*S* cinchona−enamine. It is apparent that the latent chiral information in phosphoramidite and cinchona, present in the form of stereochemical configurations, exerts a direct control over the transition-state energies and hence the stereochemistry of the ensuing product. The stereoelectronic factors behind the above-mentioned energy ordering of these crucial C−C bond formation transition states is analyzed next.

3. Interaction Wheel Model and the Origin of Stereodivergence. In order for effective chirality transfer, such as that in a stereocontrolling transition state or even in the context of a simpler chiral recognition between two molecules, two or more interactions are necessary.[46] Such critical interactions and the differential thereof are pivotal to successful chiral recognition/transfer. Herein, we propose a multipoint interaction analysis of the stereocontrolling transition states by using a concise *interaction wheel* model (Figure 5). The wheel is generated by carefully examining all the important intramolecular interactions present in the transition states. These interactions are the categorized as belonging to $\pi\cdots\pi$, C−H$\cdots\pi$, lone pair$\cdots\pi$, N$\cdots$H, and Cl$\cdots$H. Distinction is made by using an appropriate color as shown in Figure 5. Topological analyses of the electron densities have been valuable toward probing these interactions. While the topological analysis within the Atoms-In-Molecule (AIM) formalism[26] provided insights on the bond paths and bond critical points, noncovalent interaction index (NCI)[27] using the reduced density gradient could shed light on the nature of interactions.[47]

The key advantage of this representation is that it allows the readers to develop a quick grasp on the number and type interactions present in various stereocontrolling transition states, without having to go through the specifics of relatively complex geometries. However, it should be noted that the graphical model, as given, is not meant to offer a direct quantitative assessment on these interactions. Lesser number of highly favorable interactions could even outweigh a larger number of weaker interactions. Certain broad features are conspicuous, (i) the lowest energy transition states in each catalyst combination has a fully filled interaction wheel (more number of interactions) whereas the other higher energy ones is only partially filled, (ii) stereochemically complementary pairs (e.g., *re*−*si* in **P1−C1** and *si*−*re* in **P2−C2**) exhibit similar

DOI: 10.1021/jacs.5b05902
J. Am. Chem. Soc. 2015, 137, 15712−15722

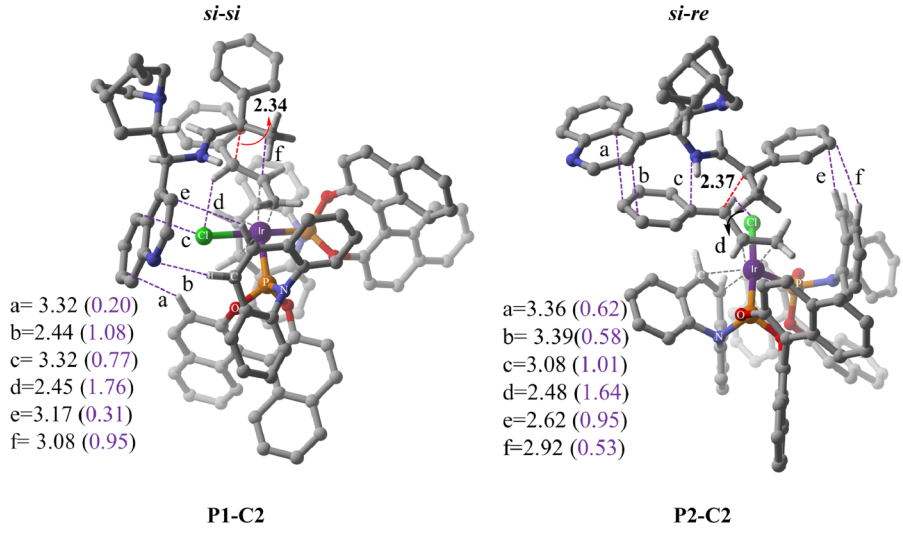

Figure 7. Optimized geometries of the stereocontroling transition states in the case of **P1−C2** and **P2−C2** catalyst combinations leading to the major stereoisomer. For improved clarity, TCA counterion and a few hydrogen atoms are omitted. Bond lengths are in angstroms. Values in parentheses are electron densities at the bond critical points along the bond paths (ρ*10^{-2} au).

type of interactions. The catalyst combination dictates the number and type of noncovalent interactions in the stereocontrolling transition states, which in turn, exerts a pivotal control over the energetic ordering responsible for the stereodivergence.

The emphasis is now placed on a representative group of stereocontrolling C−C bond formation transition states in the case of **P1−C1** catalyst dyad (Figure 6). In the present case, the origin of the large energy difference between the transition states for the *re*−*si* and *si*−*re* modes is established by probing the electronic features in greater detail. The most critical interaction is identified as emanating from the quinoline arm attached to the chiral carbon atom of the cinchona that participates in interesting π-stacking interactions with the phenyl ring of the allylic substrate (denoted as a−c in Figure 6). Similarly, a couple of crucial C−H···π contacts between the azepine olefinic C−H and the phenyl ring of the enamine (e and f) are as well identified. The electron densities at the bond critical points (ρ_{bcp}) along the bond paths for these interactions, as obtained using the AIM formalism, are given in parentheses. The ρ_{bcp} values indicate that these transition states exhibit a series of differential noncovalent interactions.

In the higher energy *si*−*si* mode of addition (Figure 6), the quinolone ring does not interact with the electrophilic allyl moiety. In this mode, responsible for the formation of (2*S*,3*R*) diastereomer, a fewer number of stabilizing interactions are noticed. Interestingly, a π-stacking (l) and a C−H···π contact (k) between the allyl and the enamine phenyl rings are present in this transition state.[48] Further analysis of the stereocontrolling transition states were performed using the *Activation Strain* model, wherein the *distortion energy* of each of the reacting partner at the transition state is computed with respect to the native undistorted reactant(s) and the *interaction energy* between such distorted reactants are then estimated.[49] The distortions in both *endo*-Ir−π-allyl and cinchona−enamine are found to be the lowest in the *re*−*si* addition, whereas the *si*−*re* exhibited the largest distortion. The extent of total distortion (i.e., sum of distortions in the reactants) are in line with the relative energy order of the corresponding transition states, suggesting that in the higher energy transition states, the reacting partners get increasingly more distorted. More importantly, the distortion in the nucleophilic enamine fragment is generally found to be lower as compared to that in the electrophilic Ir−π-allyl moiety. The distortion is primarily centered on the binaphthyl region of the chiral phosphoramidite.[50] These attributes can be regarded as a clue that modifying the phosphoramidite framework might help in steering the stereochemical outcome of the reaction.

Another interesting feature relating to the role of quinoline ring becomes evident upon comparing the most preferred mode of C−C bond formation involving other catalyst combinations such as in **P1−C2** and **P2−C2** as shown in Figure 7. In the case of **P1−C1** presented earlier, the quinoline ring participates in a π-stacking interaction in the lowest energy mode of addition. Nearly identical π-stacking interaction can also be found with **P2−C2** shown below. However, in the case of the **P1−C2** catalyst combination, the quinoline ring primarily acts as an acceptor of C−H···π interaction. Interestingly, the C−H···π interaction in this case is between cinchona and phosphoramidite, rather than between the substrate (allyl) and the catalyst (cinchona).

The molecular-level insights on the stereocontrolling transition states presented in the above sections, particularly the noncovalent interactions between different groups, could be useful toward improving the scope and efficiency of this group of cooperative catalytic reactions. Suitable choice of modified phosphoramide ligands on the Ir−π-allyl complex can make a direct effect on the enantioselectivity of the reaction. The diastereoselectivity is controlled by the nature of interactions emanating from the quinoline ring of the cinchona catalyst. Modifications on the quinoline, such introducing an electronically active substituents, could have an impact on the diastereoisomer as in the lower energy transition state quinoline engages in important interactions with the π-allyl moiety of the substrate. In the lower energy transition state, C−H···π interaction involving the olefinic C−H bonds of benzazipine and substrate aryl group (or with the quinoline ring) is also noticed. Hence this interaction involving the labile benzazipine olefin could as well be modulated by suitable substitution or by appropriate choice of substrates. On the substrate front, introduction of aryl groups could have a role in steering the stereochemical course of this reaction.

DOI: 10.1021/jacs.5b05902
J. Am. Chem. Soc. 2015, 137, 15712−15722

CONCLUSIONS

We have addressed a fundamental problem of chiral induction in asymmetric catalysis when two chiral catalysts act together in a reaction. The origin of high precision enantio- and diastereoselectivity in a cooperative dual-catalytic α-allylation of 2-phenylpropionaldehyde is established through transition-state modeling by using density functional theory (B3LYP-D3). An interesting stereoconvergence has been identified in the formation of the iridium−π-allyl intermediate wherein both *R* and *S* enantiomers of the racemic alcohol yields a single diastereomer, depending on the chirality of the phosphoramidite. The insights on controlling factors leading to stereodivergence is gathered by examining all combinations of catalyst dyads, namely, *R* or *S* Ir-phosphoramidite in conjunction with (8*R*,9*R*) or (8*S*,9*S*) cinchona amine. The reactants 2-phenylpropionaldehyde and the allyl alcohol are, respectively, activated by cinchona amine and Ir−phosphoramidite in the form of an enamine and an Ir−π-allyl intermediate. The reaction between the activated substrates produces two vicinal chiral quaternary(α) and tertiary(β) carbon atoms. With Ir−(*R*)-phosphoramidite as the catalyst, an *endo*-Ir-π-allyl intermediate is found to be energetically more favored, which reacts with the cinchona−enamine to render an *R* configuration to the β carbon. The configuration of the β carbon is decided in the formation of Ir−π-allyl intermediate. Through the multipoint contact analysis for chiral induction performed on the transition states, the quinoline ring at the C8 chiral carbon of cinchona−enamine is identified to play a direct and anchoring role in relative stabilization of the stereocontrolling transition states. The diastereoselectivity depends on the differential interactions in the C−C bond formation transition state. The success of high enantio- and diastereoselectivities relies on how independent these events are in the mechanistic course. This is a valuable insight that could help in the development of newer catalytic approaches using two chiral catalysts.

ASSOCIATED CONTENT

Supporting Information

The Supporting Information is available free of charge on the ACS Publications website at DOI: 10.1021/jacs.5b05902.

Optimized geometries, additional schemes, figures, and tables (description of mechanistic features, structural details of the transition states, topological analysis of electron densities in support of the weak noncovalent interactions) (PDF)
Movie S1 (MPG)

AUTHOR INFORMATION

Corresponding Author

*sunoj@chem.iitb.ac.in

Notes

The authors declare no competing financial interest.

ACKNOWLEDGMENTS

B.B. acknowledges a senior research fellowship from the University Grants Commission (UGC, New Delhi). The SpaceTime supercomputing facility at IIT Bombay is gratefully acknowledged for providing generous computing time. Some insightful and constructive remarks by one of the anonymous reviewers is also acknowledged.

REFERENCES

(1) Agranat, I.; Caner, H.; Caldwell, J. *Nat. Rev. Drug Discovery* **2002**, *1*, 753.
(2) LaPlante, S. R.; Fader, L. D.; Fandrick, K. R.; Fandrick, D. R.; Hucke, O.; Ray, K.; Miller, S. P. F.; Edwards, P. J. *J. Med. Chem.* **2011**, *54*, 7005.
(3) Walsh, P. J.; Kozlowski, M. C. *Fundamentals of Asymmetric Catalysis*; University Science Books: Sausalito, 2008.
(4) (a) Trost, B. M.; Crawley, M. L. *Chem. Rev.* **2003**, *103*, 2921. (b) Trost, B. M.; Lee, C. B. In *Catalytic Asymmetric Synthesis II*; Ojima, I., Ed.; Wiley-VCH: Weinheim, 2000; pp 593−650.
(5) (a) List, B. *Chem. Rev.* **2007**, *107*, 5413. (b) MacMillan, D. W. C. *Nature* **2008**, *455*, 304. (c) Knowles, R. R.; Jacobsen, E. N. *Proc. Natl. Acad. Sci. U. S. A.* **2010**, *107*, 20678.
(6) (a) Sammis, G. M.; Danjo, H.; Jacobsen, E. N. *J. Am. Chem. Soc.* **2004**, *126*, 9928. (b) Nicewicz, D. A.; MacMillan, D. W. C. *Science* **2008**, *322*, 77.
(7) Chen, D.-F.; Han, Z.-Y.; Zhou, X.-L.; Gong, L.-Z. *Acc. Chem. Res.* **2014**, *47*, 2365.
(8) (a) Kisan, H. K.; Sunoj, R. B. *J. Org. Chem.* **2015**, *80*, 2192. (b) Jindal, G.; Kisan, H. K.; Sunoj, R. B. *ACS Catal.* **2015**, *5*, 480.
(9) (a) Huang, Y.; Walji, A. M.; Larsen, C. H.; MacMillan, D. W. C. *J. Am. Chem. Soc.* **2005**, *127*, 15051. (b) Nojiri, A.; Kumagai, N.; Shibasaki, M. *J. Am. Chem. Soc.* **2009**, *131*, 3779. (c) Rana, N. K.; Huang, H.; Zhao, J. C.-G. *Angew. Chem., Int. Ed.* **2014**, *53*, 7619. (d) Oliveira, M. T.; Luparia, M.; Audisio, D.; Maulide, N. *Angew. Chem., Int. Ed.* **2013**, *52*, 13149.
(10) (a) Ibrahem, I.; Córdova, A. *Angew. Chem., Int. Ed.* **2006**, *45*, 1952. (b) Zhong, C.; Xiaodong; Shi, X. *Eur. J. Org. Chem.* **2010**, *2010*, 2999. (c) Deng, Y.; Kumar, S.; Wang, H. *Chem. Commun.* **2014**, *50*, 4272.
(11) (a) Xie, J.-Wu; Chen, W.; Li, R.; Zeng, M.; Du, W.; Yue, L.; Chen, Y.-C.; Wu, Y.; Zhu, J.; Deng, J.-G. *Angew. Chem., Int. Ed.* **2007**, *46*, 389. (b) Marcelli, T. *WIREs Comput. Mol. Sci.* **2011**, *1*, 142. (c) Melchiorre, P. *Angew. Chem., Int. Ed.* **2012**, *51*, 9748.
(12) (a) Takeuchi, R.; Kashio, M. *Angew. Chem., Int. Ed. Engl.* **1997**, *36*, 263. (b) Janssen, J. P.; Helmchen, G. *Tetrahedron Lett.* **1997**, *38*, 8025. (c) Bartels, B.; Helmchen, G. *Chem. Commun.* **1999**, 741. (d) Tissot-Croset, K.; Polet, D.; Alexakis, A. *Angew. Chem., Int. Ed.* **2004**, *43*, 2426. (e) *Transition Metal Catalyzed Enantioselective Allylic Substitutions in Organic Synthesis*; Kazmaier, U., Ed.; Springer: Berlin, 2012.
(13) (a) Roggen, M.; Carreira, E. M. *J. Am. Chem. Soc.* **2010**, *132*, 11917. (b) Roggen, M.; Carreira, E. M. *Angew. Chem., Int. Ed.* **2011**, *50*, 5568. (c) Roggen, M.; Carreira, E. M. *Angew. Chem., Int. Ed.* **2012**, *51*, 8652. (d) Hamilton, J. Y.; Sarlah, D.; Carreira, E. M. *J. Am. Chem. Soc.* **2013**, *135*, 994. (e) Krautwald, S.; Schafroth, M. A.; Sarlah, D.; Carreira, E. M. *J. Am. Chem. Soc.* **2014**, *136*, 3020. (f) Ruchti, J.; Carreira, E. M. *J. Am. Chem. Soc.* **2014**, *136*, 16756. (g) Hartwig, J. F.; Stanley, L. M. *Acc. Chem. Res.* **2010**, *43*, 1461. (h) Hartwig, J. F.; Stanley, L. M. *Acc. Chem. Res.* **2010**, *43*, 1461. (i) Stanley, L. M.; Bai, C.; Ueda, M.; Hartwig, J. F. *J. Am. Chem. Soc.* **2010**, *132*, 8918. (j) Madrahimov, S. T.; Hartwig, J. F. *J. Am. Chem. Soc.* **2012**, *134*, 8136. (k) Chen, W.; Hartwig, J. F. *J. Am. Chem. Soc.* **2012**, *134*, 15249. (l) Chen, W.; Hartwig, J. F. *J. Am. Chem. Soc.* **2014**, *136*, 377. (m) Chen, W.; Chen, M.; Hartwig, J. F. *J. Am. Chem. Soc.* **2014**, *136*, 15825. (n) Chen, M.; Hartwig, J. F. *Angew. Chem., Int. Ed.* **2014**, *53*, 12172. (o) Raskatov, J. A.; Jäkel, M.; Straub, B. F.; Rominger, F.; Helmchen, G. *Chem. - Eur. J.* **2012**, *18*, 14314. (p) Qu, J.; Roßberg, L.; Helmchen, G. *J. Am. Chem. Soc.* **2014**, *136*, 1272. (q) Liu, W.-B.; Zheng, C.; Zhuo, C.-X.; Dai, L.-X.; You, S.-Li. *J. Am. Chem. Soc.* **2012**, *134*, 4812.
(14) Krautwald, S.; Sarlah, D.; Schafroth, M. A.; Carreira, E. M. *Science* **2013**, *340*, 1065.
(15) (a) Shinisha, C. B.; Sunoj, R. B. *J. Am. Chem. Soc.* **2010**, *132*, 12319. (b) Sharma, A. K.; Sunoj, R. B. *Angew. Chem., Int. Ed.* **2010**, *49*, 6373. (c) Simón, L.; Goodman, J. M. *J. Am. Chem. Soc.* **2012**, *134*, 16869. (d) Sladojevich, F.; de Arriba, A. L. F.; Ortín, I.; Yang, T.; Ferrali, A.; Paton, R. S.; Dixon, D. J. *Chem. - Eur. J.* **2013**, *19*, 14286.

DOI: 10.1021/jacs.5b05902
J. Am. Chem. Soc. 2015, 137, 15712−15722

(e) Grayson, M. N.; Goodman, J. M. *J. Am. Chem. Soc.* **2013**, *135*, 6142. (f) Yang, H.; Wong, M. W. *J. Am. Chem. Soc.* **2013**, *135*, 5808. (g) Jindal, G.; Sunoj, R. B. *Angew. Chem., Int. Ed.* **2014**, *53*, 4432. (h) Watson, C. G.; Balanta, A.; Elford, T. G.; Essafi, S.; Harvey, J. N.; Aggarwal, V. K. *J. Am. Chem. Soc.* **2014**, *136*, 17370. (i) Lam, Y.-H.; Houk, K. N. *J. Am. Chem. Soc.* **2015**, *137*, 2116. (j) Reddi, Y.; Sunoj, R. B. *ACS Catal.* **2015**, *5*, 1596. (k) Jindal, G.; Sunoj, R. B. *Org. Lett.* **2015**, *17*, 2874.

(16) (a) Shinisha, C. B.; Sunoj, R. B. *Org. Biomol. Chem.* **2007**, *5*, 1287. (b) Young, K. J. H.; Oxgaard, J.; Ess, D. H.; Meier, S. K.; Stewart, T.; Goddard, W. A., III; Periana, R. A. *Chem. Commun.* **2009**, 3270. (c) Cheong, P. H.-Y.; Legault, C. Y.; Um, J. M.; Çelebi-Ölçüm, N.; Houk, K. N. *Chem. Rev.* **2011**, *111*, 5042. (d) Cheng, M.-J.; Fu, R.; Goddard, W. A., III *Chem. Commun.* **2014**, *50*, 1748. (e) Lam, Y.-H.; Houk, K. N. *J. Am. Chem. Soc.* **2014**, *136*, 9556. (f) Jindal, G.; Sunoj, R. B. *Org. Biomol. Chem.* **2014**, *12*, 2745.

(17) Frisch, M. J.; Trucks, G. W.; Schlegel, H. B.; Scuseria, G. E.; Robb, M. A.; Cheeseman, J. R.; Scalmani, G.; Barone, V.; Mennucci, B.; Petersson, G. A.; Nakatsuji, H.; Caricato, M.; Li, X.; Hratchian, H. P.; Izmaylov, A. F.; Bloino, J.; Zheng, G.; Sonnenberg, J. L.; Hada, M.; Ehara, M.; Toyota, K.; Fukuda, R.; Hasegawa, J.; Ishida, M.; Nakajima, T.; Honda, Y.; Kitao, O.; Nakai, H.; Vreven, T.; Montgomery, J. A., Jr.; Peralta, J. E.;Ogliaro, F.; Bearpark, M.; Heyd, J. J.; Brothers, E.; Kudin, K. N.; Staroverov, V. N.; Kobayashi, R.; Normand, J.; Raghavachari, K.; Rendell, A.; Burant, J. C.; Iyengar, S. S.; Tomasi, J.; Cossi, M.; Rega, N.; Millam, N. J.; Klene, M.; Knox, J. E.; Cross, J. B.; Bakken, V.; Adamo, C.; Jaramillo, J.; Gomperts, R.; Stratmann, R. E.; Yazyev, O.; Austin, A. J.; Cammi, R.; Pomelli, C.; Ochterski, J. W.; Martin, R. L.; Morokuma, K.; Zakrzewski, V. G.; Voth, G. A.; Salvador, P.; Dannenberg, J. J.; Dapprich, S.; Daniels, A. D.; Farkas, Ö.; Foresman, J. B.; Ortiz, J. V.; Cioslowski, J.; Fox, D. J. *Gaussian 09, Revision A.02*; Gaussian, Inc.: Wallingford, CT, 2013.

(18) Grimme, S.; Antony, J.; Ehrlich, S.; Krieg, H. *J. Chem. Phys.* **2010**, *132*, 154104.

(19) (a) Hay, P. J.; Wadt, W. R. *J. Chem. Phys.* **1985**, *82*, 270. (b) Hay, P. J.; Wadt, W. R. *J. Chem. Phys.* **1985**, *82*, 299.

(20) (a) Gonzalez, C.; Schlegel, H. B. *J. Chem. Phys.* **1989**, *90*, 2154. (b) Gonzalez, C.; Schlegel, H. B. *J. Phys. Chem.* **1990**, *94*, 5523.

(21) Marenich, A. V.; Cramer, C. J.; Truhlar, D. G. *J. Phys. Chem. B* **2009**, *113*, 6378.

(22) (a) Weigend, F.; Ahlrichs, R. *Phys. Chem. Chem. Phys.* **2005**, *7*, 3297. (b) Weigend, F. *Phys. Chem. Chem. Phys.* **2006**, *8*, 1057.

(23) (a) Lee, C.; Yang, W.; Parr, R. G. *Phys. Rev. B: Condens. Matter Mater. Phys.* **1988**, *37*, 785. (b) Becke, A. D. *Phys. Rev. A: At., Mol., Opt. Phys.* **1988**, *38*, 3098. (c) Becke, A. D. *J. Chem. Phys.* **1993**, *98*, 5648.

(24) Zhao, Y.; Truhlar, D. G. *Theor. Chem. Acc.* **2008**, *120*, 215.

(25) Legault, C. Y. *CYLview, 1.0 b*; Université de Sherbrooke, Quebec, Canada, 2009 (http://www.cylview.org).

(26) (a) Bader, R. F. W. *Chem. Rev.* **1991**, *91*, 893. (b) *AIM2000 Version 2.0*; Buro fur Innovative Software, SBK-Software: Bielefeld, Germany, 2002. (c) Matta, C. F.; Boyd. R. J. *Quantum Theory of Atoms in Molecules: Recent Progress in Theory and Application*; Wiley-VCH: Weinheim, 2007.

(27) (a) Johnson, E. R.; Keinan, S.; Mori-Sánchez, P.; Contreras-García, J.; Cohen, A. J.; Yang, W. *J. Am. Chem. Soc.* **2010**, *132*, 6498. (b) Contreras-García, J.; Johnson, E. R.; Keinan, S.; Chaudret, R.; Piquemal, J. − P.; Beratan, D. N.; Yang, W. *J. Chem. Theory Comput.* **2011**, *7*, 625.

(28) (a) Balcells, D.; Maseras, F. *New J. Chem.* **2007**, *31*, 333. (b) Goodman, J. M.; Kirby, P. D.; Haustedt, L. O. *Tetrahedron Lett.* **2000**, *41*, 9879.

(29) Full details on the energetics of formation of enamine intermediate are provided in Figures S4−S9 and Scheme S5 in the Supporting Information.

(30) For additional details on the conformational sampling of cinchona and cinchona enamine, see Figures S4 and S11 in the Supporting Information.

(31) Defieber, C.; Grützmacher, H.; Carreira, E. M. *Angew. Chem., Int. Ed.* **2008**, *47*, 4482.

(32) Computed Gibbs free energies for different active species are provided in Table S1, Figure S1, and Scheme S2 in the Supporting Information.

(33) Linden, A.; Dorta, R. *Acta Crystallogr., Sect. C: Cryst. Struct. Commun.* **2010**, *C66*, m290.

(34) More details of the conformational and configuration search are provided in Figure S10 in the Supporting Information.

(35) See Scheme S3 in the Supporting Information for more details. A similar observation was earlier noted by Huo et al. See: Huo, X.; Yang, G.; Liu, D.; Liu, Y.; Gridnev, I. D.; Zhang, W. *Angew. Chem., Int. Ed.* **2014**, *53*, 6776.

(36) (a) See Figure S6 in the Supporting Information for an additional illustration. (b) Moran, A.; Hamilton, A.; Bo, C.; Melchiorre, P. *J. Am. Chem. Soc.* **2013**, *135*, 9091.

(37) See Scheme S4 and Figure S2 in the Supporting Information for more details on shape selectivity.

(38) It should be noted that the face of the π-allyl moiety binding with the iridium center is different in $\mathbf{c}_R$ and $\mathbf{c}'_R$. These should be regarded as two different configurations as they are not interconvertible through simple rotations around the C−C single bond.

(39) (a) The elementary step barrier with respect to the preceding intermediate, as obtained through the intrinsic reaction coordinate calculations, also conveys the same trend.. (b) The geometric and energetic details of TCA-assisted dehydroxylation from the $\mathbf{c}'_S$ configuration of $[IrCl(\mathbf{P1})_2]$ *S*-allyl alcohol complex is provided in Figure S16 in the Supporting Information..

(40) (a) Additional details are provided in Figure S17 in the Supporting Information.

(41) (a) See Figure S18 in the Supporting Information for the geometry of the transition state.. (b) Earlier experimental studies on *endo*−*exo* interconversions in Ir−π-allyl species suggested that it is unlikely under the normal reaction conditions. See refs 12c and 13a,c,i,j. (c) Ito, H.; Kunii, S.; Sawamura, M. *Nat. Chem.* **2010**, *2*, 972. (d) Ariafard, A.; Bi, S.; Lin, Z. *Organometallics* **2005**, *24*, 2241.

(42) See Scheme S1 in the Supporting Information for an additional illustration.

(43) See Figures S12 and S13 in the Supporting Information for more details.

(44) See Scheme S6, Figures S14 and S15, and Table S2 in the Supporting Information for more details.

(45) (a) Krenske, E. H.; Houk, K. N.; Lohse, A. G.; Antoline, J. E.; Hsung, R. P. *Chem. Sci.* **2010**, *1*, 387. (b) Zhang, W.; Zhu, Y.; Wei, D.; Li, Y.; Tang, M. *J. Org. Chem.* **2012**, *77*, 10729.

(46) (a) Davankov, V. A. *Chirality* **1997**, *9*, 99. (b) Kühnle, A.; Linderoth, T. R.; Hammer, B.; Besenbacher, F. *Nature* **2002**, *415*, 891.

(47) Additional details of AIM and NCI plots are provided, respectively, in Figure S19, Table S3, and Movie S1 in the Supporting Information.

(48) An increasing number of examples are now available that emphasize noncovalent interactions as a key contributing factor to enantioselectivity in asymmetric catalysis. See: (a) Krenske, E. H.; Houk, K. N. *Acc. Chem. Res.* **2013**, *46*, 979. (b) Wheeler, S. E. *Acc. Chem. Res.* **2013**, *46*, 1029. (c) Lu, T.; Wheeler, S. E. *Science* **2015**, *347*, 719. (d) See refs 8a and 15g.

(49) More details are provided in Figure S20 and Table S4 in the Supporting Information. (a) Bickelhaupt, F. M. *J. Comput. Chem.* **1999**, *20*, 114. (b) van Zeist, W.-J.; Bickelhaupt, F. M. *Org. Biomol. Chem.* **2010**, *8*, 3118. (c) Zheng, C.; Zhuo, C.-X.; You, S.-L. *J. Am. Chem. Soc.* **2014**, *136*, 16251.

(50) See Figure S21 in the Supporting Information for more details.

NOTE ADDED AFTER ASAP PUBLICATION

This paper was published ASAP on 12/04/2015 with an error in the Table of Contents/Abstract graphic. The corrected version was reposted on December 8, 2015.

DOI: 10.1021/jacs.5b05902
J. Am. Chem. Soc. 2015, 137, 15712−15722